Available online at www.sciencedirect.com
ScienceDirect
Geochimica et Cosmochimica Acta 71 (2007) 3311–3322
Geochimica et Cosmochimica Acta
www.elsevier.com/locate/gca

Mechanism of hydrothermal alteration of natural self-irradiated and synthetic crystalline titanate-based pyrochlore

P. Pöml [a,*], M. Menneken [a], T. Stephan [b], D.R.D. Niedermeier [a], T. Geisler [a], A. Putnis [a]

[a] Institut für Mineralogie, Westfälische Wilhelms-Universität, Corrensstraße 24, 48149 Münster, Germany
[b] Institut für Planetologie, Westfälische Wilhelms-Universität, Wilhelm-Klemm-Straße 10, 48149 Münster, Germany

Received 23 October 2006; accepted in revised form 23 March 2007; available online 13 April 2007

Abstract

Pyrochlore-based ceramics are considered as a potential host to immobilize high-level nuclear waste in a geological repository. For this application it is essential to investigate the fundamental mechanism of the equilibration of pyrochlore in aqueous solutions. We treated cuboids of a synthetic crystalline and a natural metamict, i.e., self-irradiation-damaged Ti-based pyrochlore in 1 ml of a 1 M HCl solution containing 43.5% ^{18}O at 250 °C for 72 h. After the experiments the colours of the samples turned from black to almost white and their surfaces were covered by micron-sized crystallites. Both samples were mainly transformed into rutile with subordinate anatase and the reaction can be traced several tens of micrometers into the cuboids. In the case of the natural pyrochlore an additional phase (aeschynite [$(REE)(Ti,Nb)_2(O,OH)_2$]) appeared as crystals on the surface and within an up to 100 μm thick layer at the interface between TiO_2 and the unreacted pyrochlore. ^{18}O is in both cases highly enriched in the reaction products with a sharp gradient (on a micrometer scale) to the unreacted pyrochlore. The replacement reaction retains even fine-scale morphological features typical for pseudomorphs. This observation along with the enrichment of ^{18}O in the product phases and the textural features clearly show that the dissolution of pyrochlore is spatially coupled with the precipitation of stable (metastable) TiO_2 phases at a moving front. During such a coupled process dissolution at the proceeding front is the rate controlling step. The aeschynite phase at the interface is thought to be either an intermediate alteration product or crystallized from a fluid which is located at the interface between the TiO_2 polymorphs and the unreacted pyrochlore due to changing transport properties between the interface and the fluid with increasing thickness of the TiO_2 rim. We emphasize here that our results produced under relatively extreme batch-experimental conditions show similarities with nature as well as with results derived from experiments conducted under moderate conditions rather expected in a nuclear repository.

1. INTRODUCTION

The disposal of highly radioactive waste is a topic of particular concern for the modern world. Actinides and fission products from the nuclear fuel cycle, high-level waste (HLW) from reprocessing to reclaim fissile materials for energy production, and plutonium from either the production or dismantlement of nuclear weapons are radioactive materials that have to be disposed of in a way to protect the public and the environment. A recent overview of the amounts of waste waiting to be disposed of and the general strategy for handling can be found in Ewing (2006). Apart from the already existing amount of plutonium (≈1855 metric tons at the end of 2003, Albright and Kramer (2004)) the global inventory of plutonium continues to increase by approximately 70–100 tons/year. This plutonium is either still incorporated in spent nuclear fuel or already separated by the reprocessing of commercial nuclear fuel. The latter amount reached ≈300 metric tons in the year 2000 and is thus greater than the amount of plutonium presently

* Corresponding author. Fax: +49 251 8338397.
E-mail address: philipp@poeml.de (P. Pöml).

0016-7037/$ - see front matter © 2007 Elsevier Ltd. All rights reserved.
doi:10.1016/j.gca.2007.03.031

incorporated in nuclear weapons (in 1998 about ≈252 metric tons, see Stoll, 1998 for details). Hence, the peaceful use of nuclear energy will inevitably require a strategy for the disposal of actinides and particularly fissile ^{239}Pu. However, many countries do not want to develop a strategy for the disposal of these actinides, but rather prefer that they, in particular Pu, will be burned in fast reactors. This is the strategy that is pursued in the U.S. and Russia and is inherent in the present Global Nuclear Energy Partnership. In addition to the plutonium and uranium, "minor" actinides such as ^{237}Np, ^{241}Am + ^{243}Am, and ^{244}Cm are generated in reactors, and global production rates are 3.4, 2.7, and 0.35 metric tons per year, respectively. For the disposal of wastes containing these isotopes the currently accepted strategy is the vitrification in a borosilicate glass matrix. However, it is well known that glass is not a thermodynamically stable material. Because isotopes like ^{239}Pu (half-life = 24,100 a) and ^{237}Np (half-life = 2,100,000 a) are long lived isotopes, the radiotoxicity of ^{239}Pu, ^{237}Np, and their fission products will be a risk over geological time scales (10^5–10^6 a). Another problem of equal importance is the generally low solubility of actinides in borosilicate glasses. Waste loadings of no more than 2% are probably all that can be achieved. Therefore, other materials have been proposed for the immobilisation and disposition of plutonium. Of special interest are ceramics made from, e.g., pyrochlore, zirconolite, baddeleyite, zircon, or monazite, which are minerals that are well known for their durability, i.e., they persist as placer deposits in stream beds after surviving sometimes several cycles of weathering, erosion, transport, and deposition. A very popular ceramic assemblage proposed as a nuclear waste form is SYNROC (Ringwood et al., 1988), a mixture of zirconolite, perovskite, hollandite, and rutile. These potential waste forms are thought to be more stable than nuclear waste forms made from glass and have been subject of numerous studies (see, e.g., Ringwood et al., 1979, 1988; Lumpkin et al., 1994; Ewing et al., 1995). Pyrochlore structure-type materials are also promising candidates as potential host phases for actinides (Ewing et al., 2004; Ewing, 2005). There are hundreds of different pyrochlore-structured compositions, several of them including actinides (Chakoumakos and Ewing, 1985), and in nature pyrochlores are also common in highly evolved rock types like pegmatites and carbonatites. Compositions containing uranium and thorium, as well as transuranium elements (e.g., Pu, Cm) have been synthesized. Natural pyrochlore samples can contain up to 30 wt% UO_2 and 9 wt% ThO_2.

Currently, two laboratory approaches are used for studying the aqueous durability of potential nuclear waste form materials. The first approach involves so-called flow-through "leaching" experiments. The aim of these flow-through experiments is to gain information about the dissolution rates as usually measured by element release rates of the examined materials. In a flow-through experiment the fluid is continuously transported away from the sample while fresh fluid is supplied. Due to this fluid flow supersaturation with respect to new phases can usually be avoided. In contrast to this, the second approach involves so-called "closed-system" or "batch" experiments. In this type of experiment, the tested sample is treated for a specific time at a certain temperature in a fixed amount of fluid. In such an experimental arrangement new stable phases have, after partial dissolution of the sample, the chance to precipitate, resulting in a gradual change of the fluid composition with time. There is an ongoing debate about the significance of data gained from either laboratory approach for evaluating the long-time performance of potential nuclear waste form materials and whether kinetic data obtained in the laboratory can be extrapolated to physicochemical conditions of natural systems.

In this study we carried out two hydrothermal batch experiments involving ^{18}O as a tracer. The first sample treated was a synthetic pyrochlore with a composition of a possible nuclear waste ceramic containing Gd and Hf as neutron absorbers and Ce as a surrogate for a real waste load of Pu. The second sample was a natural, ≈1 Gyr old pyrochlore, a betafite-(Y) containing approximately 11 wt% UO_2. Because of the decay of U this sample has accumulated a high degree of radiation damage over the past million years—thus simulating the radiation damage synthetic samples, containing a nuclear waste load, will accumulate over time. Both samples were treated under the same conditions. The aim of these experiments using ^{18}O was to gain information about the alteration mechanisms, the impact of radiation damage on the aqueous durability, and to investigate whether the results of batch experiments under extreme conditions can be applied to natural systems to predict the long-term stability of pyrochlore.

2. METHODS

2.1. Analytical methods

2.1.1. Powder X-ray diffractometry (XRD)

Powder X-ray diffraction data were obtained with a Philips X'Pert automated diffractometer using monochromatic Cu-Kα_1 radiation ($\lambda = 1.5406$ Å). The operating conditions were 40 kV acceleration voltage at 30 nA tube current. The samples were scanned with a step-size of 0.02° (2θ) from 10 to 60° (2θ). The counting times were 8 and 90 s for sample PS1 and P4, respectively. The instrument was calibrated using silicon as an external standard.

2.1.2. Scanning electron microscopy (SEM)

Backscattered electron (BSE) images, energy dispersive X-ray (EDX) mappings, and EDX semi-quantitative analyses were acquired with a JEOL 840 scanning electron microscope at 20 kV acceleration voltage. For both BSE images and EDX analysis the beam current was adjusted in order to get the best possible contrast and counting statistics. High-resolution secondary electron (SE) pictures of the samples' surfaces were obtained using a JEOL JSM 6300F equipped with a field emission gun and operated at 1 kV acceleration voltage.

2.1.3. Electron probe micro-analysis (EPMA)

Both the starting materials and the experimental run products were quantitatively analysed by electron probe micro-analysis (EPMA) using a JEOL JXA 8600 MX Superprobe operated at 20 kV acceleration voltage and 15 nA

beam current. These conditions result in a lateral resolution of 2–4 μm, depending on the element analysed (Reed, 1975). As standards natural minerals and synthetic compounds were used: a natural diopside for Ca and Si, synthetic phosphates for Y and the rare earth elements (REE), a natural rutile for Ti, a synthetic zircon for Zr, synthetic oxides for Nb and Ta, a synthetic huttonite for Th, UO_2 for U, a natural rhodonite for Mn, a natural hematite for Fe, and a Pb–Zn glass for Pb. The ZAF correction procedure was applied to correct for matrix effects.

2.1.4. Time-of-flight secondary ion mass spectrometry (TOF-SIMS)

The TOF-SIMS mapping data were acquired using an ION-TOF TOF-SIMS IV mass spectrometer. During the analysis the two samples were bombarded with a pulsed 25 keV Ga^+ primary ion beam (pulse width 1.5 ns). Prior to the analysis the samples were sputter-cleaned with 3 keV argon ions. A fine-focused gallium beam with a diameter of ≈300 nm was subsequently rastered over an area of 235×235 and 300×300 μm^2 for sample PS1 and P4, respectively. For both samples 256×256 pixels were recorded. For each pixel, entire mass spectra were determined for both polarities in two consecutive measurements. The $^{18}O/(^{16}O + ^{18}O)$ ratio could be quantified directly from the number of counts since only a single detector is used and matrix effects have little effect on isotope ratios. More details of the TOF-SIMS technique are described elsewhere (Stephan, 2001).

2.1.5. Confocal μ-Raman spectroscopy

For phase and polytype identification a high-resolution Jobin Yvon HR800 Raman spectrometer utilizing a Nd–YAG (532 nm) laser was used. The scattered Raman light was collected in both cases in 180° backscattering geometry and dispersed by a grating of 1800 groves/mm after having passed a 150 μm entrance slit. A $100 \times$ objective (NA = 0.9) and a confocal hole of 400 μm was used for all measurements.

2.2. Hydrothermal experiments

For the hydrothermal experiments a polished cuboid was prepared from the starting material of each sample. By defining the shape of the samples used for the experiments, we were able to monitor the textural changes during the hydrothermal treatment, which is difficult when working with powders. For the synthetic pyrochlore the dimension of the cuboid was $3.3 \times 3.4 \times 3.3$ mm^3 and the weight was 179.65 mg. The natural pyrochlore weighed 191.2 mg and had the dimension of $3.3 \times 3.4 \times 3.4$ mm^3. Using an UP193HE Excimer laser with a beam diameter of 12 μm, the letters "WWU" were engraved into the surface of each sample. This was done in order to be able to also investigate

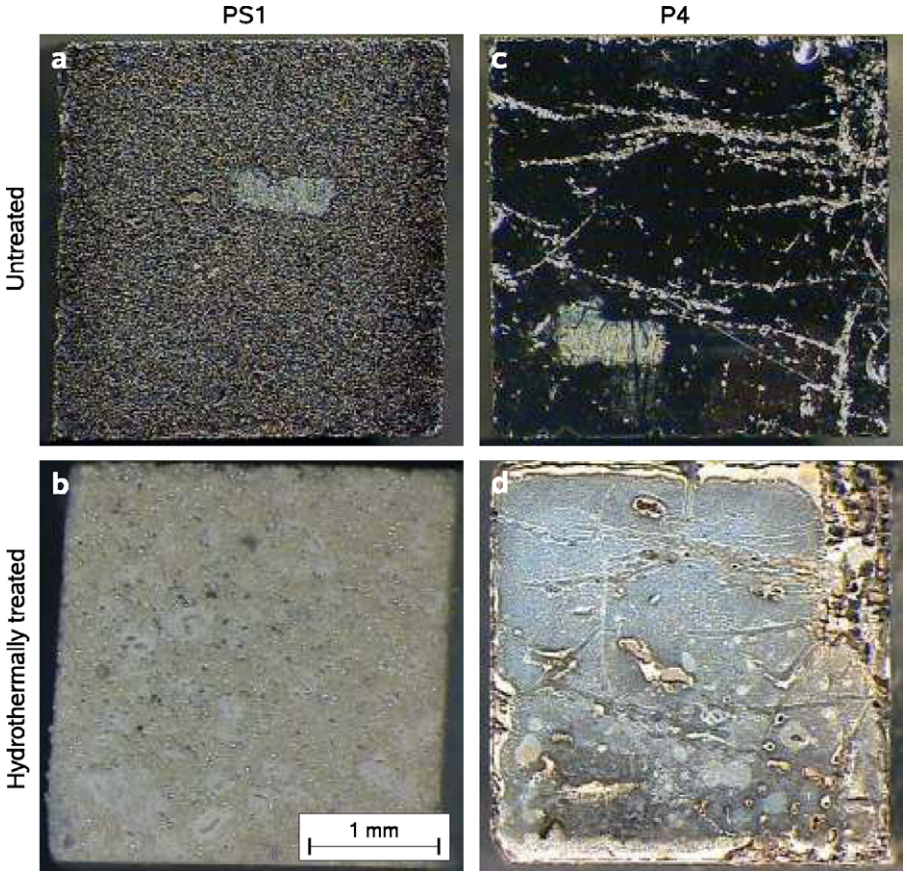

Fig. 1. Optical micrographs showing the cuboids prepared from the synthetic pyrochlore PS1 and the natural pyrochlore P4. (a) and (c) show the cuboids before hydrothermal treatment, while (b) and (d) show the cuboids after treatment. The bright areas on the surfaces of the cuboids in (a) and (c) mark the locations where the letters "WWU" were engraved.

whether fine-scale morphological features will be retained or lost during the hydrothermal treatment. Optical micrographs of the two cuboids with the engraved letters are shown in Fig. 1a and c.

Each cuboid was then placed in a cold-sealed silver reactor (3 cm^3 volume) and 1.06 ml of a 1.09 M HCl solution containing 43.5% ^{18}O was added into each reactor. The samples were then treated for 72 h at 250 ± 1 °C.

3. SAMPLE CHARACTERISATION

3.1. Synthetic crystalline pyrochlore (PS1)

The pyrochlore PS1 is a synthetic crystalline ceramic made at the Lawrence Livermore National Laboratory (USA) and was kindly provided by B. Burakov. The ceramic consists of a Ti-based pyrochlore (grain sizes between 8 and 60 μm) as the major phase with minor amounts of perovskite and rutile as revealed by XRD (Fig. 2). The chemical compositions of all three phases are listed in Table 1. The empirical structural formula of the pyrochlore is

$$(Ca_{0.76}Ce_{0.75}Gd_{0.23}Hf_{0.21})Ti_2O_7$$

(B. Burakov, personal communication). The optical micrograph of the polished surface of the cuboid used for the experiment reveals a relative high degree of porosity of the ceramic (Fig. 1a). Note that the bright area on the surface of the cuboid marks the area where the letters "WWU" were engraved. The porosity is also seen in a SE image from the area enclosing the engraved letters (Fig. 3a). Note that the SE images of the untreated cuboids were made without carbon coating.

3.2. Natural self-irradiated pyrochlore (P4)

The natural sample P4 is a X-ray amorphous Y-enriched betafite from a rare earth pegmatite from Lindvigskollen near Kragerø, South Norway. The sample was provided by the Mineralogical Museum of the University of Hamburg, Germany. The XRD spectrum shows no Bragg diffraction peaks. Instead two broad humps appear at approximately 30° and 50° (2θ) (Fig. 2), which are typical for metamict pyrochlore. Nevertheless, we have heated the sample to 1000 °C to be able to confirm that the sample had indeed a pyrochlore structure. Unfortunately, the material recrystallized to uranopolycrase. Powder of the sample was analysed by transmission electron microscopy (TEM). Most recorded electron diffraction patterns show broad rings from the amorphous phase, but diffraction patterns from some areas additionally show diffraction rings composed of diffraction spots, which demonstrate the occurrence of relict crystalline domains, which are randomly oriented. The diffraction rings could unambiguously be assigned to pyrochlore. The occurrence of crystalline remnants indicates that different areas have suffered a different degree of self-irradiation damage. The average cumulated α-decay dose for an age of 1020 ± 10 Ma is $(38.7 \pm 4.2) \times 10^{19}$ α-decays/g (see Geisler et al. (2005c)). Such heterogeneity is also reflected by EPMA measurements. Apart from some chemical and structural heterogeneity, the sample also shows natural primary alteration features (Geisler et al., 2005c). The average chemical composition of the unaltered areas derived from 146 EPM-analyses yield the following empirical structural formula (Table 1):

$$(Y_{0.52}REE_{0.23}U_{0.16}Ca_{0.07}Fe_{0.06}Th_{0.04}Pb_{0.03}\square_{0.89})\quad (Ti_{1.24}Nb_{0.69}Ta_{0.05}Zr_{0.01})_{\Sigma=2}O_{6.05}\square_{0.95}\cdot 0.65\ H_2O,$$

where REE are rare earth elements (Lu, Ho, Nd, Tb, Dy, Er, and Yb). □ represents a vacancy.

To avoid any superimposition of the natural alteration on the experimental alteration, we prepared a number of cuboids from the sample and selected a cuboid that did not show any alteration features in reflected light. An optical micrograph of the selected cuboid is shown in Fig. 1c. Fig. 3d shows a SE image of the polished surface of this cuboid with the engraved letters.

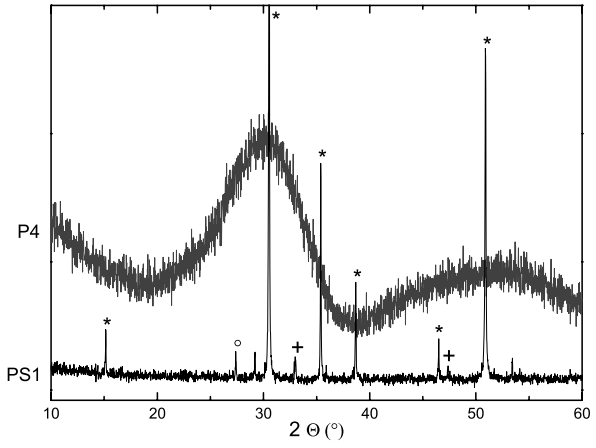

Fig. 2. Powder X-ray diffraction profiles of the synthetic pyrochlore PS1 and the natural pyrochlore P4. The latter sample is clearly amorphous. To make the broad humps for the P4 sample more visible, the XRD data were multiplied with an appropriate factor. The characters "∗", "+", and "∘" mark diffraction peaks belonging to pyrochlore, perovskite, and rutile, respectively.

4. RESULTS

4.1. Synthetic crystalline pyrochlore (PS1)

Fig. 1b shows an optical micrograph of the cuboid of the synthetic sample PS1 after the experiment. By comparing this image with that shown in Fig. 1a, it is apparent that the shape of the cuboid remained the same, but that the colour turned from black to white. The engraved letters "WWU" are optically not visible anymore. However, the letters "WWU" are still recognisable in a SE image (Fig. 3b), although the surface structure changed dramati-

Table 1
Average chemical compositions (in wt%) of the phases observed in this study

n	PS1				P4			
	Starting material[a]			Altered Zones	Staring material	Altered zones		
	Pyrochlore 3	Perovskite 3	Rutile/anatase 2	Rutile/anatase 4[c]	Pyrochlore[b] 146	Aeschynite 45	Rutile/anatase 2[c]	U-phase 2[c]
CaO	10.02	19.86	4.10	0.1	0.96	0.65		
CeO_2	29.42	24.22	5.83	0.7	0.15	0.26		
Gd_2O_3	10.24	5.56	1.60		1.33	1.58		
TiO_2	38.14	48.65	75.80	76.9	25.76	22.43	36.7	32.3
HfO_2	12.18	1.71	12.68	22.3				
ZrO_2	<0.1				0.37	0.34		
Nb_2O_5					23.72	27.33	41.2	10.4
Ta_2O_5					2.96	3.02	5.7	
SiO_2					0.06	0.38		
ThO_2					2.70	2.60		
UO_2					11.14	7.07	14.3[e]	54.1
Y_2O_3					15.19	15.78	0.5	
$\sum$REE[d]					9.59	10.47		
MnO					0.04	0.03		
FeO					1.17	0.52	0.8	
PbO					1.83	0.67		
Total	100	100	100	100	96.97	93.13	99.2	96.8
H_2O[f]						6.89		

Data were derived from *n* electron probe micro-analyses or as noted from *n* semi-quantitative EDX analyses.
[a] Data from B. Burakov, personal communication.
[b] Unaltered pyrochlore.
[c] Semi-quantitative EDX analyses.
[d] The analysed REE are Lu, Ho, Nd, Tb, Dy, Er, and Yb.
[e] It is not clear whether U was incorporated in anatase/rutile or is bound in small crystallites of aeschynite and/or the U-phase which are intergrown with anatase and rutile.
[f] H_2O is calculated as the difference between the total and 100 wt%.

cally. The surface is now covered by numerous small crystals, resulting in a rough surface morphology. In higher magnifications, SE imaging reveals two different types of crystal habits, i.e., a dominating bipyramidal and a minor tabular habit, as well as a bimodal crystal size distribution (Fig. 3c). One population of crystals is about 4.5 μm in size, whereas the second population of crystals measures only about 0.6 μm on average. Raman measurements revealed that the crystals at the surface are mainly composed of the TiO_2 polymorph rutile and subordinate anatase (Fig. 4).

Fig. 5a and b show BSE images of a cross section of the cuboid, which reveal four zones of different microtexture and BSE intensity. The core zone, marked with a "1" in Fig. 5, represents the completely unreacted part of the sample. The second zone "2" shows the same average BSE intensity than the core area, but a slightly, yet noteworthy increased porosity. Around this high-porosity area a transitional zone "3" with a slightly darker BSE contrast developed, resulting from the occurrence of rutile and anatase along with unaltered pyrochlore remnants. The outermost zone "4" shows the darkest BSE contrast and the highest porosity with very few pyrochlore relicts. The transition between zone "3" and "4" is gradual. The overall replacement area, including the zones "2", "3", and "4", has an average width of about 1000 μm.

Fig. 6 shows results of the EDX and TOF-SIMS mapping along with a BSE image of a selected area from the transitional zone between zones "3" and "4", which is marked in Fig. 5b. It is apparent that Ca, Gd, and Ce were not incorporated into the reaction product in significant amounts and thus must be lost to the fluid phase. This is also confirmed by semi-quantitative EDX analyses of the rutile/anatase mixture. These analyses additionally reveal that the TiO_2 polymorphs incorporated only significant amounts of Hf (Table 1), which was, as Gd, included in the baseline formulation of the pyrochlore as a neutron absorber. From the TOF-SIMS distribution of ^{18}O (displayed as the $^{18}O/(^{16}O + ^{18}O)$ ratio) it is apparent that the TiO_2 reaction products are strongly enriched in heavy oxygen. Since the Raman spectra of the TiO_2 polymorphs produced during the experiment show a significant red shift of the fundamental bands when compared to reference spectra from rutile and anatase of normal oxygen isotope composition (Fig. 4), such enrichment is due to the incorporation of ^{18}O in the framework structure of the polymorphs rather than due to any water that can potentially be incorporated in rutile formed in a hydrothermal environment (Swope et al., 1995).

4.2. Natural self-irradiated pyrochlore (P4)

Fig. 1d shows an optical micrograph of the cuboid of the natural sample P4 after the experiment. Like the cuboid of the treated synthetic sample, the surface colour of the cuboid from sample P4 turned into milky-white. When compared with the image of the starting material (Fig. 1c), it is noticeable that the cracks are still visible. However, the

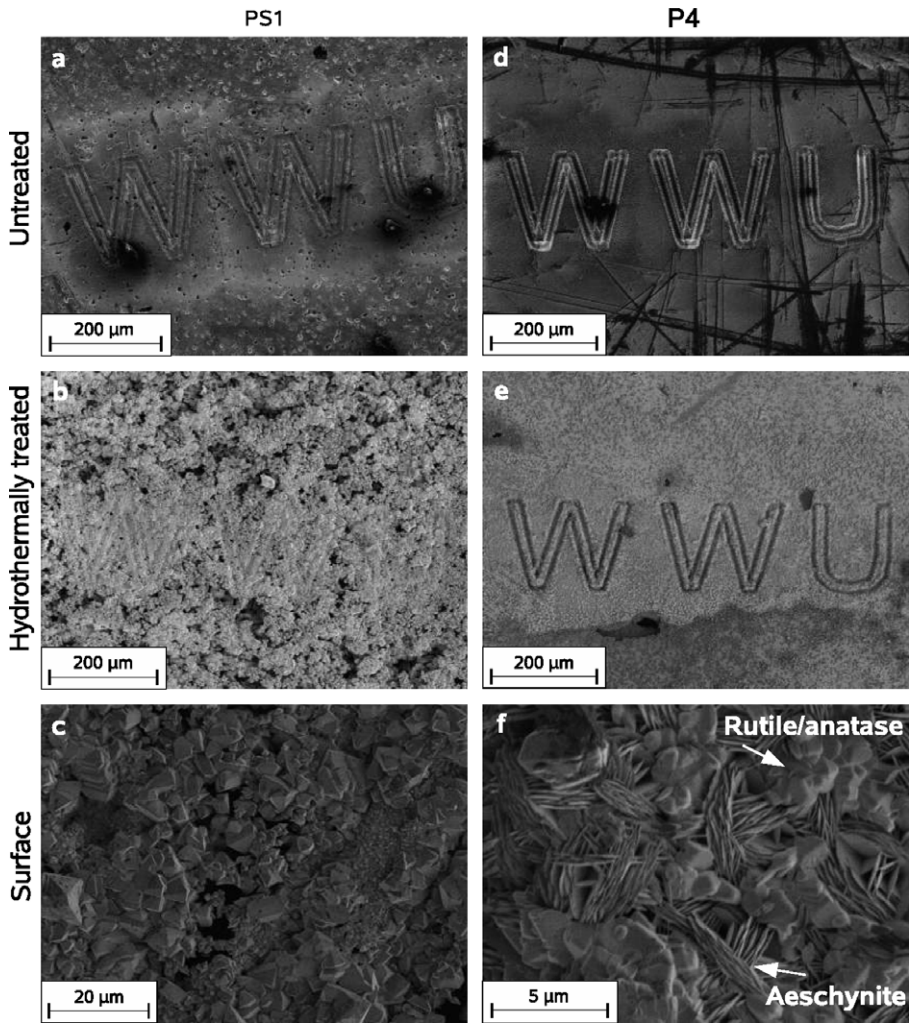

Fig. 3. Secondary electron images of the surfaces of (a) and (d) the untreated samples PS1 and P4, respectively, and (b) and (e) the treated sample surfaces of both samples. The surface of the synthetic sample (b) changed dramatically. However, the letters "WWU" are still readable. Only little has changed on the surface of the natural pyrochlore (e). (c) and (f) show detailed images of the PS1 and P4 surfaces. Relatively large crystals (up to 7 µm) grew on the surface of PS1, smaller crystals evolved on the P4 surface. Two different phases marked with arrows in (f) could be identified on the P4 surface.

cuboid shows slightly rounded edges. A closer look at the area of the engraved letters "WWU" reveals that changes seem to be less severe than for the synthetic pyrochlore (compare Fig. 3b and e). The edges of the engraved letters are still sharp, although the surface is covered with new crystals (Fig. 3f). This can be explained by the smaller size of the crystals when compared to the crystals covering the surface of the synthetic sample PS1. Two different crystal morphologies can be recognized on the high-resolution SE image shown in Fig. 3f. The first crystal type forms rose-like aggregates, whereas the second type of crystals shows a relative isometrical morphology with few tetragonal pyramides. The Raman spectrum of the rose-like crystals is identical to that from aeschynite $[(REE)(Ti,Nb)_2(O,OH)_2]$, whereas the spectrum from an area composed mainly of the isometrical crystals shows bands which can again be assigned to both rutile and anatase (Fig. 4).

The cross-section of the cuboid shows a different picture compared to the synthetic sample (Fig. 5c and d). The BSE image shown in Fig. 5c reveals a rim, about 100 µm wide, of low BSE intensity, which penetrates deeply into the cuboid along cracks by forming finger-like alteration zones. Another important textural feature is the broad gap that runs parallel to the surface of the cuboid and marks the interface between reaction rim and unreacted pyrochlore in those areas, which are free of the finger-like zones (marked by arrows in Fig. 5c and d). As expected, the dark rim is mainly composed of rutile with minor amounts of anatase. We note here that both polymorphs were also identified by XRD and TEM as replacement products in previous experiments with the same sample, which were carried out under similar, though not identical conditions (Geisler et al., 2005b). In the interior of the cuboid, the finger-like zones are surrounded by another phase which is only detectable by BSE imaging due to the occurrence of a high porosity, since the BSE intensity generated from these areas is indistinguishable from that generated from the unreacted pyrochlore. This phase could be identified as aeschynite by Raman spectroscopy (Fig. 4),

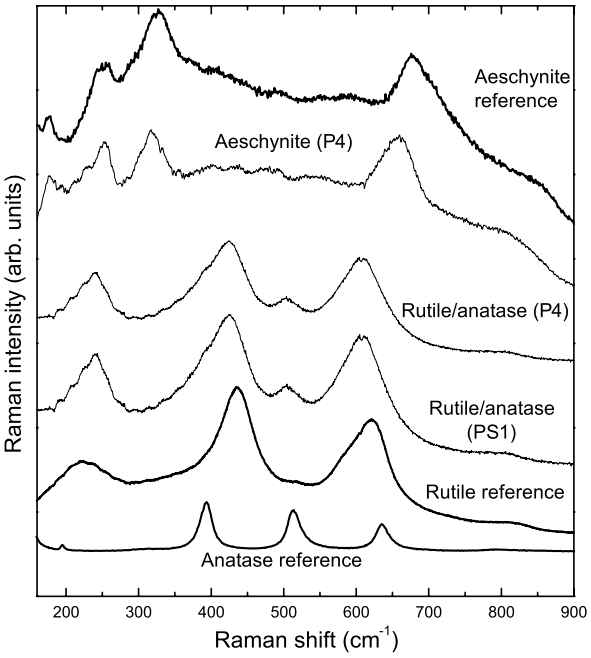

Fig. 4. Raman spectra of the alteration product of the PS1 experiment (Rutile/anatase (PS1)), the alteration products of the P4 experiment (Aeschynite (P4) and Rutile/anatase (P4)), and the reference spectra for aeschynite, rutile, and anatase. The frequency shift between the bands of the reference spectra and the spectra of the experimental crystals is due to the ^{18}O in the structure of the experimental products.

which also formed in some areas at the surface of the cuboid (Fig. 3f). EPMA measurements revealed that the aeschynite contains high amounts of rare earth elements (Table 1). Further phases can be identified in the sample at higher magnifications. These phases are visible as white spots in the BSE image shown in Fig. 6g, but also as white spots along the crack visible in Fig. 5d.

Fig. 6h–k shows element distribution maps of Nb, Ti, Y, and U from an area that is marked by a rectangle in Fig. 5d. This area was selected, because it includes a tip of an alteration finger (see Ti distribution shown in Fig. 6i), which is surrounded by aeschynite. It is apparent that the rutile/anatase assemblage is strongly enriched in Nb and U. Semi-quantitative EDX analyses yielded on average 14 wt% UO_2 and 41 wt% Nb_2O_5, as well as 5 wt% Ta_2O_5 (Table 1). The U concentration in TiO_2 is thus significantly higher than in TiO_2 formed in previous experiments under slightly different conditions, even when considering the uncertainties associated with EDX analyses. We attribute the high U content to micro- or nanometer-sized crystallites of U phases, which are embedded in TiO_2, rather than being entirely incorporated in the rutile or anatase structure. This is in agreement with the sprinkled distribution of U seen in Fig. 6k. We also note that U is enriched along the crack from which the reaction spread out. From the elemental distribution images it is apparent that these U phases contain variable amounts of U, Y, Ti, and/or Nb. The chemical composition of one analysable secondary U phase is given in

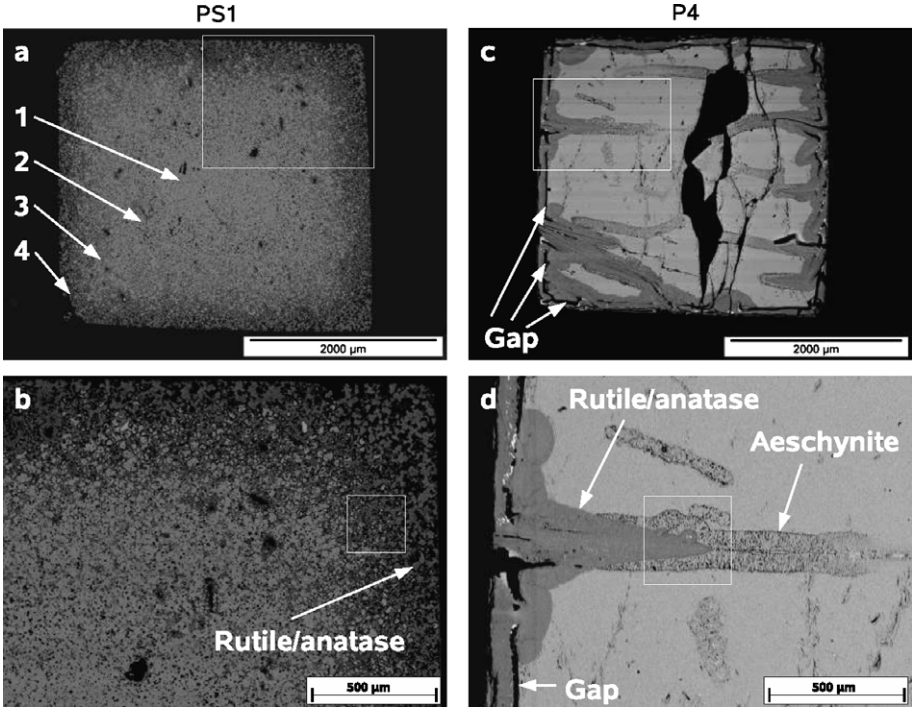

Fig. 5. BSE images of the cross sections of the cuboids. (a) and (b) show the PS1 sample. The unreacted inside of the cuboid shows a brighter BSE contrast than the altered outer rim. In (a) four different zones are marked by numbers (1)–(4). Details are given in the text. The alteration of the natural P4 sample also took place along cracks (c and d). The rectangles in (a) and (c) mark the areas shown in (b) and (d), respectively. Those in (b) and (d) mark the areas mapped by TOF-SIMS and EDX (Fig. 6).

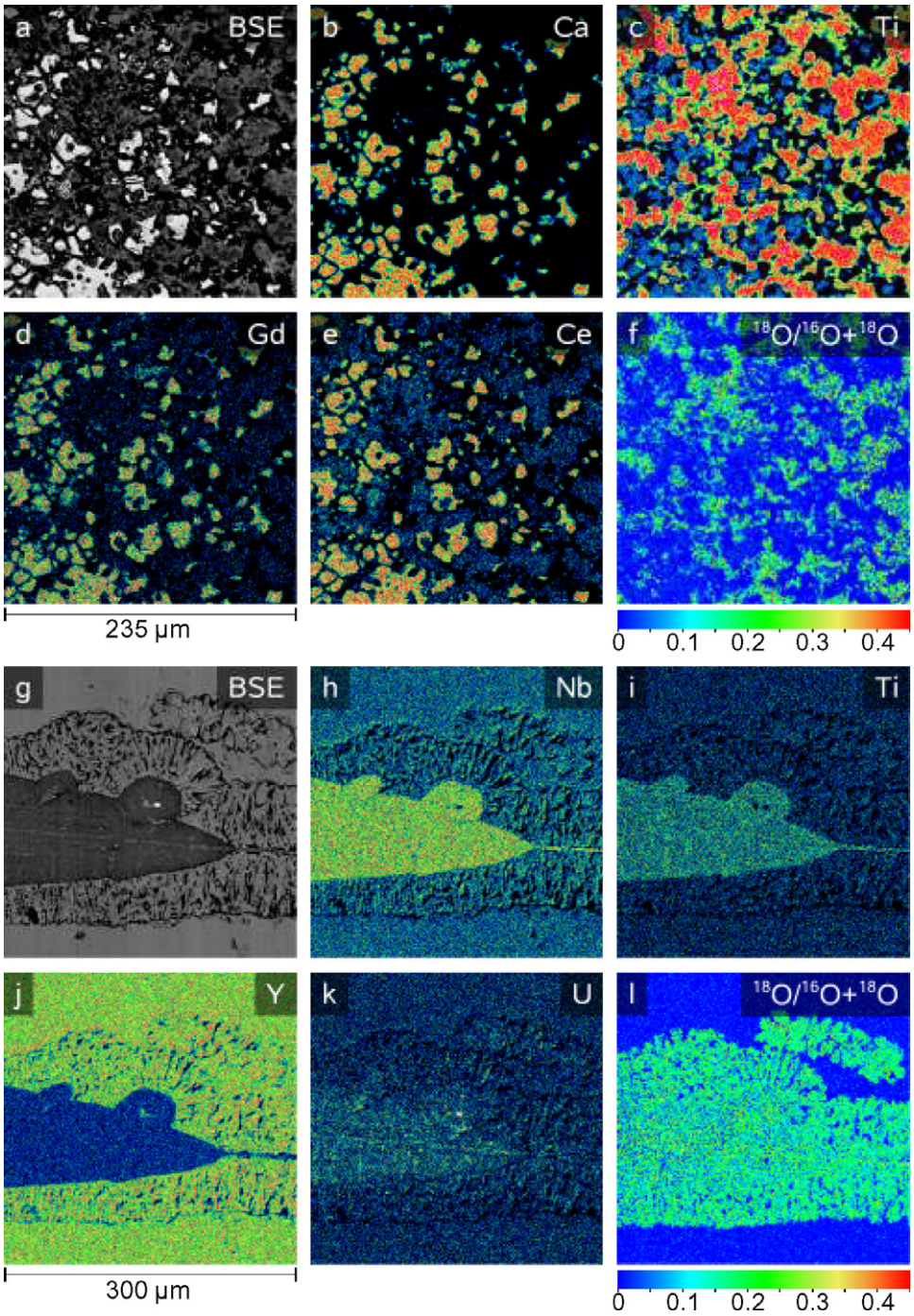

Fig. 6. (a) and (g) show BSE images of the areas analysed by EDX and TOF-SIMS mapping in PS1 and P4, respectively. Both areas are marked in Fig. 5. (b)–(e) show the distribution for the elements Ca, Ti, Gd, and Ce in the synthetic PS1 sample. (h)–(k) Element distribution maps for Nb, Ti, Y, and U in the natural P4 sample. (f) and (l) show the $^{18}O/(^{16}O + ^{18}O)$ ratio for PS1 and P4, respectively.

Table 1. As for the synthetic pyrochlore PS1, the TOF-SIMS ^{18}O distribution image reveals that ^{18}O is strongly enriched in the TiO_2 polymorphs, but also in the aeschynite phase (Fig. 6l). The ^{18}O-enrichment is due to the incorporation of ^{18}O in the framework structure rather than due to any water that can potentially be incorporated in these phases as again shown by the red shift of their fundamental Raman active vibrations (see Fig. 4). Interestingly, ^{18}O is equally distributed between the TiO_2 polymorphs and the aeschynite phase. We further note that the ^{18}O gradient between the aeschynite phase and the unreacted pyrochlore is sharp on the micrometer scale. No increase of ^{18}O in the unaltered pyrochlore is discernible.

5. DISCUSSION

5.1. Mechanism of alteration

In previous experiments with the same natural pyrochlore (P4) under similar conditions, we observed complex banding structures, which were interpreted as being the result of a diffusion–reaction process while the pyrochlore was in the solid state (Geisler et al., 2005c). We suggested that during the alteration process the REEs, Y, and most of the U were selectively removed from the amorphous betafite, leaving behind Ti, Nb, and Ta, allowing the nucleation and growth of anatase and the anatase-to-rutile transformation to occur. However, the enrichment of ^{18}O in the reaction products and the textural features observed in the present study unambiguously demonstrate that the product phases crystallized from the solution. Consequently, both the self-irradiation damaged and the crystalline pyrochlore dissolved congruently in the hydrochloric acid, because the initial solution was undersaturated with respect to pyrochlore, but then the fluid-pyrochlore interface became immediately supersaturated with respect to TiO_2. The observation that the cuboids were still intact and the engraved letters on the surfaces were still present after the experiments indicates that the dissolution of pyrochlore is also spatially coupled with the crystallization of the new product phases by retaining the initial volume of the parent phase. As discussed by Putnis (2002) such a coupling of dissolution and precipitation can result in the complete replacement of one phase by another without losing the external shape or crystal morphology of the parent phase as in pseudomorphism. The observation that the initial volume is conserved during the reaction, although the molar volumes and/or the solubilities of the parent and product phases are different, is a general observation in mineral replacement reactions (Labotka et al., 2004; Putnis and Mezger, 2004; Putnis et al., 2005). In a previous study, for example, we have experimentally altered a natural, crystalline Ta-based pyrochlore (microlite) under similar conditions (Geisler et al., 2004, 2005b,c). The results showed that the microlite was replaced by a defect pyrochlore that has an epitactic crystallographic relationship with the parent pyrochlore. In the present case, however, the parent phase is either polycrystalline or amorphous and there is no crystallographic relationship between the product and parent phases.

Both rutile and anatase have a lower molar volume than radiation-damaged and crystalline Ti-based pyrochlore (rutile/anatase ≈ 20 cm^3/mol, betafite-(Y) ≈ 83 cm^3/mol, data from webmineral.com). Furthermore, in both cases the reaction involves loss of elements to the fluid. It is clear that the external volume can only be conserved by the formation of porosity within the reaction products. A key feature for the understanding of the replacement process in the radiation-damaged natural pyrochlore is the observation of the large gap that runs parallel to the surface and marks the interface between the TiO_2 polymorphs and the unaltered pyrochlore (see Fig. 5c and d). Since the pyrochlore is almost fully amorphous, the initial nucleation of the Ta- and Nb-rich TiO_2 polymorphs onto the pyrochlore surface must have occurred randomly with no crystallographic relationship between the individual TiO_2 nuclei after a few pyrochlore surface layers dissolved. Since the entropy of the anatase-to-rutile transformation is small (Schuiling and Vink, 1967), the crystallization of anatase most likely occurred metastably, because rutile is the thermodynamically stable TiO_2 polymorph in solutions within a large temperature range. This is in agreement with the fact that nanocrystalline anatase is a common polymorph in synthetic and natural samples at low temperatures (Navrotsky, 2002). It is thus likely that anatase initially nucleated and, with particle coarsening, anatase transformed into rutile. We would like to point out here that the initial dissolution–reprecipitation step cannot have involved the complete covering of the whole pyrochlore surface due to the difference in the molar volume of the product and parent phases. Hence, the dissolution of pyrochlore could proceed once the Ti concentration at the interface solution had been decreased due to the nucleation/crystallization of TiO_2. It is clear that the next nucleation of TiO_2 occurred at the pre-existing TiO_2 crystals rather than at the inward penetrating new surface of the pyrochlore, because such an epitaxial nucleation process must be energetically advantageous when compared with the heterogeneous nucleation onto the amorphous pyrochlore surface. Due to the random crystallographic orientation of the initially formed crystals, the TiO_2 crystals form a polycrystalline layer that nonetheless retains even fine morphological details of the parent phase. We note here that the anatase/rutile replacement zone is indeed polycrystalline with a random grain orientation, as observed by TEM in our previous study (Geisler et al., 2005c). The replacement process can be understood as a transport of material through the interfacial fluid film from the pyrochlore surface to the TiO_2 layer. During such a process, the gap between the pyrochlore surface and the newly formed TiO_2 layer and thus the volume of the interfacial fluid increased. The large gap between the TiO_2 layer and the pyrochlore is thus likely the relict of such a fluid film. Since the growing TiO_2 layer also contained some porosity, the interfacial fluid was not trapped, but could communicate with the surrounding fluid.

As a result of the pre-existing cracks in the cuboid of the natural sample, the fluid could also penetrate deeper into the cuboid (Fig. 5c and d). It is apparent from Fig. 5d that the replacement reaction spread out perpendicular to the direction of these cracks, which resulted in a local closure of the gap between the TiO_2 layer and the pyrochlore. The occurrence of the aeschynite phase both as thick layers inside the cuboid and as crystallites on the surface of the cuboid is not yet fully understood. The phase could be understood as an intermediate alteration product. This would mean that the pyrochlore first recrystallized into aeschynite before it was subsequently transformed into rutile/anatase as the alteration process proceeded. The aeschynite crystals on the surface of the sample might be relicts of such an intermediate alteration product. Nevertheless, our preferred interpretation is that the aeschynite phase crystallized from an interfacial fluid between the unreacted pyrochlore and the alteration products rutile/anatase that was supersaturated with respect to aeschynite. This supersaturation could

develop as the chemical exchange between the external and interfacial fluid slowed down because of an increasing penetration of the reaction into the cuboid and a growing thickness of the TiO_2 layer. If this was the case, the occurrence of thick layers of aeschynite crystals inside the cuboid is a direct evidence for an increasing deviation from equilibrium between the external and the interfacial fluid. Although our Raman measurement did not reveal the occurrence of aeschynite inside the TiO_2 layer, it is likely that the fluid inside the porous TiO_2 layer was also locally supersaturated with respect to aeschynite. This would also explain the occurrence of aeschynite at the surface of the cuboid. We note here that aeschynite was not found throughout the surface, but is concentrated in certain regions. These regions might be associated with cracks that are exposed to the surface.

The observations made for the synthetic sample PS1 are slightly different due to its polycrystalline character. Here, the fluid could migrate into the sample along the grain boundaries and through the open space given by the primary porosity. No clear reaction front can be traced on the large scale, but a closer look reveals many partly replaced pyrochlore grains that were attacked by the fluid migrating along the grain boundaries (Fig. 6a). TEM investigations are necessary to study the crystallographic relationship between anatase/rutile and pyrochlore. Interestingly, the zone "2" around the unaltered core is characterized by a significantly increased porosity when compared to the primary porosity of the ceramic (Fig. 5a). This increase in porosity indicates that the Ti was not directly re-precipitated as TiO_2 inside the ceramic, but was first transported from this central zone further to the outside. The reason for this is currently unknown.

An important consequence of the coupling between dissolution and reprecipitation for the evaluation of the stability of pyrochlore is that the replacement is independent from the absolute solubility of pyrochlore and its replacement products in the solution. The driving force for the replacement reaction is merely the relative difference between the solubility of pyrochlore and the TiO_2 product phases. Since the replacement zone is characterised by the existence of porosity or grain boundaries, the TiO_2 rim cannot be considered as a protective layer.

5.2. Impact of self-irradiation structural damage

It is still a major issue whether amorphous pyrochlore is more prone to alteration than the crystalline counterpart. Begg et al. (2001), for example, have not found any difference between the dissolution rate of amorphised and crystalline $Y_2Ti_2O_7$ and $Gd_2Ti_2O_7$ pyrochlore compositions. Icenhower et al. (2006) and Strachan et al. (2005) presented data that suggest that there is no increase in dissolution rate as a result of a radiation damage. However there are also data available that show a 50-fold increase in the element release rate of Cm-doped amorphous titanate pyrochlores (Weber et al., 1986). Since the synthetic pyrochlore is polycrystalline and the natural pyrochlore sample was a large single crystal (now amorphous) with no apparent grain boundaries, it is difficult to compare the overall extent of the replacement reaction. Compared to the natural sample the reaction advanced deeper into the crystalline sample, because the ceramic is polycrystalline and the fluid could thus migrate into the sample along grain boundaries. However, the grain size of the ceramic ranges between 8 and 60 μm in diameter. Even close to the surface of the cuboid not all pyrochlore grains are completely replaced by TiO_2, which means that the reaction would probably not have advanced deeper than about 10–30 μm in the case of a single crystal (note that the grains were attacked from all sides). This would be less than half the thickness of the replacement zone observed in the natural radiation-damaged sample, indicating that the dissolution of pyrochlore (and the reprecipitation of TiO_2) was faster in the radiation-damaged pyrochlore. This could also explain the observation that the TiO_2 crystals at the surface of this sample are significantly smaller than those at the surface of the crystalline ceramic (compare Fig. 3c and f), because fast dissolution resulted in high supersaturation at the interface and thus in a high nucleation rate, i.e., there was less time for the TiO_2 crystals to grow before more nuclei formed.

5.3. Relevance of this study for nuclear waste immobilization in pyrochlore

The main question that immediately arises when considering the relevance of our study for nuclear waste immobilization in pyrochlore is whether batch experiments made with solutions having an extreme proton activity are relevant for the assessment of what will happen with a pyrochlore waste form in a nuclear repository when it comes in contact with an aqueous fluid. This question has been answered indirectly by many researchers, who tried to address this issue and carried out their experiments under moderate conditions (low temperature, low proton or hydroxide activity, low salinity) that are expected in a potential nuclear waste repository. Often flow-through experiments are conducted to be able to determine the rate of dissolution of pyrochlore (e.g., Roberts et al., 2000; Icenhower et al., 2006). These approaches are reasonable and certainly valuable to the problem. However, due to the moderate conditions, reaction rates are often very slow so that changes in the solid occur merely at the nanoscale and the mechanism of reequilibration is thus difficult to investigate (e.g., Leturcq et al., 2001). As a consequence, the information on the mechanism is mainly obtained by analysing the experimental fluid and modelling the system by equilibrium models. The approach of the present study is completely different and relates to the question of the long-term performance of a pyrochlore waste form under geological conditions. In this and other studies (see Geisler et al., 2004, 2005a,b,c) we accelerated the mineral-fluid equilibration by using an extreme proton activity in our starting solution, which hardly occurs on Earth and, least of all, in a potential nuclear repository. By doing this we are, in principle, able to investigate what will happen with a pyrochlore that is exposed to natural aqueous solutions over geological time scales, if we are able to show that our results on the mechanism of mineral-fluid re-equilibration are independent on the proton activity and that the observations made in our

experiments agree to some extent with those made on natural samples.

It is a well-known fact that an increase of the proton activity does not only increase the rate of dissolution, but may also change phase equilibria. However, the occurrence of rutile/anatase has been reported as a breakdown product of naturally altered pyrochlore samples (Lumpkin, 2001). Furthermore, Zhang et al. (2004) reported the formation of TiO_2 at the surface of $Y_2Ti_2O_7$ pyrochlore treated statically in a 0.001 M NaF solution with a pH of 2 at 90 °C for 4 weeks. Anatase was also observed by Begg et al. (2001) at the surface of $Y_2Ti_2O_7$ and $Gd_2Ti_2O_7$ pyrochlores, after being treated in a nitric acid solution with a pH of 2 at 90 °C. These observations are supported by (1) numerous dissolution studies under various conditions, which have shown that the solution chemistry does not reflect the stoichiometry of the investigated pyrochlore, which is believed to be the result of non-stoichiometric dissolution (e.g., Roberts et al., 2000) and (2) by the extremely low solubility of TiO_2 phases in acidic and basic solutions in a wide temperature range (Ayers and Watson, 1993; Knauss et al., 2001). These data suggest that TiO_2 is a breakdown product of Ti-based pyrochlore over a wide range of physicochemical conditions and we can conclude that neither the extreme proton activity of our solution nor the elevated temperature of 250 °C is responsible for the formation of TiO_2. The formation of other replacement products such as aeschynite and the U phases observed in the experiment with the natural pyrochlore, however, may depend on the pH. It is clear that the question of the formation of U (or Pu) phases is relevant for modelling the near-field of a repository, which can potentially be designed as to buffer a potential aqueous solution infiltrating the repository.

The next question that we have raised is whether results of a batch experiment can be transferred to nature. Previous mineralogical studies on the alteration of natural pyrochlore-group minerals have shown that pyrochlores found in heavily weathered rock, e.g., in laterites, show typical features of replacement reactions (e.g., Lottermoser and England, 1988; Lumpkin and Ewing, 1992, 1995, 1996; Williams et al., 1997; Nasraoui et al., 1999; Nasraoui and Bilal, 2000; Lumpkin, 2001; Lumpkin et al., 2001). The pyrochlore crystals investigated in these studies are characterised by replacement zones that irregularly penetrated into the crystals, i.e., they obviously survived during weathering rather than being dissolved. In recent studies we could show that the chemical and structural characteristics of the replacement zones found in natural Ta-based (microlite) pyrochlore could be reproduced under batch experimental conditions using a 1 M HCl solution (Geisler et al., 2004, 2005b,c). It could further be demonstrated by ^{18}O tracer experiments and transmission electron microscopy that the observed features are fully consistent with a coupled dissolution–reprecipitation process rather than with a solid state process involving volume diffusion. It is thus reasonable to conclude that the flow of the natural fluids, which have altered the pyrochlore crystals, was not fast enough to transport elements away from the solid-fluid interface. Consequently, after the initial step of dissolution, the immediate supersaturation of the stable product phase(s) could occur. Nature has obviously designed batch experiments. In these "experiments" the kinetics of the replacement process were fast when compared with the transport of ions in the natural fluid.

Finally, we conclude that Ti-based pyrochlore is thermodynamically not stable in an aqueous solution under most, if not all, *P–T–X* conditions prevailing in the Earth's crust. Based on our results, we suggest that it should be possible to reliably predict the long-term stability of a pyrochlore waste form in a nuclear repository by measuring the kinetics of the replacement process in batch experiments at different proton activities, salinities, and temperatures. The experimental conditions can be chosen as to be able to quantitatively measure the replacement process with analytical techniques available today. It is clear that the analysis of the fluid will provide important complementary data to determine the kinetics of the process.

ACKNOWLEDGMENTS

We are indebted to J. Schlüter from the Mineralogical Museum of the University of Hamburg and B. Burakov for providing the natural and synthetic pyrochlore samples, respectively. The difficult and time-consuming preparation of the polished cuboids of the samples by Uli Böcker is gratefully acknowledged. Arne Janßen is thanked for his help with the XRD measurements. We also thank Rodney C. Ewing and Jonathan P. Icenhower for their very friendly and helpful reviews. We further acknowledge financial support by the Deutsche Forschungsgemeinschaft (Grant GE 1094/5) and the European Commission (ACTINET Grant 03-02).

REFERENCES

Albright D., and Kramer K. (2004) Stockpiles still growing. *Bull. Atom. Sci.* **60**, 14–16.

Ayers J. C., and Watson E. B. (1993) Rutile solubility and mobility in supercritical aqueous fluids. *Contrib. Mineral. Petrol.* **114**, 321–330.

Begg B. D., Hess N. J., Weber W. J., Devanathan R., Icenhower J. P., Thevuthasan S., and McGrail B. P. (2001) Heavy-ion irradiation effects on structures and acid dissolution of pyrochlores. *J. Nucl. Mater.* **288**, 208–216.

Chakoumakos B. C., and Ewing R. C. (1985) Crystal chemical constraints on the formation of actinide pyrochlores. In *Scientific Basis for Nuclear Waste Management VIII*, vol. 44 (eds. C. M. Jantzen, J. A. Stone, and R. C. Ewing). Materials Research Society, Pittsburgh, Pennsylvania, pp. 641–646.

Ewing R. C. (2005) Plutonium and "minor" actinides: safe sequestration. *Earth Planet. Sci. Lett.* **229**, 165–181.

Ewing R. C. (2006) The nuclear fuel cycle: A role for mineralogy and geochemistry. *Elements* **2**, 331–334.

Ewing R. C., Weber, W. J., and Lutze W. (1995). In *Disposal of Weapon Plutonium Approaches and Prospects* (eds. E.R. Merz and C.E. Walter). Kluwer, Dordrecht, The Netherlands, pp. 65–83.

Ewing R. C., Weber W. J., and Lian J. (2004) Nuclear waste disposal—pyrochlore ($A_2B_2O_7$): Nuclear waste form for the immobilization of plutonium and "minor" actinides. *J. Appl. Phys.* **95**, 5949–5971.

Geisler T., Berndt J., Meyer H. W., Pollok K., and Putnis A. (2004) Low-temperature aqueous alteration of crystalline pyrochlore: correspondence between nature and experiment. *Mineral. Mag.* **68**, 905–922.

Geisler T., Burakov B., Yagovkina M., Garbuzov V., Zamoryanskaya M., Zirlin V., and Nikolaeva L. (2005a) Structural recovery of self-irradiated natural and ^{238}Pu-doped zircon in an acidic solution at 175 °C. *J. Nucl. Mater.* **336**, 22–30.

Geisler T., Pöml P., Stephan T., Janssen A., and Putnis A. (2005b) Experimental observation of an interface-controlled pseudomorphic replacement reaction in a natural crystalline pyrochlore. *Am. Mineral.* **90**, 1683–1687.

Geisler T., Seydoux-Guillaume A. M., Poeml P., Golla-Schindler U., Berndt J., Wirth R., Pollok K., Janssen A., and Putnis A. (2005c) Experimental hydrothermal alteration of crystalline and radiation-damaged pyrochlore. *J. Nucl. Mater.* **344**, 17–23.

Icenhower J. P., Strachan D. M., McGrail B. P., Scheele R. D., Rodriguez E. A., Steele J. L., and Legore V. L. (2006) Dissolution kinetics of pyrochlore ceramics for the disposition of plutonium. *Am. Mineral.* **91**, 39–53.

Knauss K. G., Dibley M. J., Bourcier W. L., and Shaw H. F. (2001) Ti(IV) hydrolysis constants derived from rutile solubility measurements made from 100 to 300 °C. *Appl. Geochem.* **16**, 1115–1128.

Labotka T. C., Cole D. R., Fayek M., Riciputi L. R., and Stadermann F. J. (2004) Coupled cation and oxygen-isotope exchange between alkali feldspar and aqueous chloride. *Am. Mineral.* **89**, 1822–1825.

Leturcq G., Advocat T., Hart K., Berger G., Lacombe J., and Bonnetier A. (2001) Solubility study of Ti,Zr-based ceramics designed to immobilize long-lived radionuclides. *Am. Mineral.* **86**, 871–880.

Lottermoser B. G., and England B. M. (1988) Compositional variation in pyrochlores from the Mt Weld carbonatite laterite, Western Australia. *Mineral. Petrol.* **38**, 37–51.

Lumpkin G. R. (2001) Alpha-decay damage and aqueous durability of actinide host phases in natural systems. *J. Nucl. Mater.* **289**, 136–166.

Lumpkin G. R., and Ewing R. C. (1992) Geochemical alteration of pyrochlore group minerals: Microlite subgroup. *Am. Mineral.* **77**, 179–188.

Lumpkin G. R., and Ewing R. C. (1995) Geochemical alteration of pyrochlore group minerals: Pyrochlore subgroup. *Am. Mineral.* **80**, 732–743.

Lumpkin G. R., and Ewing R. C. (1996) Geochemical alteration of pyrochlore group minerals: Betafite subgroup. *Am. Mineral.* **81**, 1237–1248.

Lumpkin G. R., Hart K. P., McGlinn P. J., Payne T. E., Gieré R., and Williams C. T. (1994) Retention of actinides in natural pyrochlores and zirconolites. *Radiochimi. Acta*(66/67), 469–474.

Lumpkin G. R., Ewing R. C., Williams C. T., and Mariano, A. N. (2001) An overview of the crystal chemistry, durability, and radiation damage effects of natural pyrochlore. In *Scientific Basis for Nuclear Waste Management XXIV*, vol. 663 (eds. K. P. Hart and G. R. Lumpkin). Materials Research Society, Warrendale, Pennsylvania, pp. 921–934.

Nasraoui M., and Bilal E. (2000) Pyrochlores from the Lueshe carbonatite complex (Democratic Republic of Congo): a geochemical record of different alteration stages. *J. Asian Earth Sci.* **18**, 237–251.

Nasraoui M., Bilal E., and Gibert R. (1999) Fresh and weathered pyrochlore studies by Fourier transform infrared spectroscopy coupled with thermal analysis. *Mineral. Mag.* **63**, 567–578.

Navrotsky A. (2002) Thermochemistry, energetic modelling and systematics. In *Energy Modelling in Minerals*, vol. 4 of *EMU Notes in Mineralogy* (ed. C. M. Gramaccioli). Eötvös University Press, Budapest, pp. 5–31, Chapter 2.

Putnis A. (2002) Mineral replacement reactions: from macroscopic observations to microscopic mechanisms. *Mineral. Mag.* **66**, 689–708.

Putnis C. V., and Mezger K. (2004) A mechanism of mineral replacement: Isotope tracing in the model system KCl–KBr–H_2O. *Geochim. Cosmochim. Acta* **68**, 2839–2848.

Putnis C. V., Tsukamoto K., and Nishimura Y. (2005) Direct observations of pseudomorphism: compositional and textural evolution at a fluid–solid interface. *Am. Mineral.* **90**, 1909–1912.

Reed S. J. B. (1975) *Electron Microprobe Analysis*. Cambridge University Press, Cambridge, UK.

Ringwood A. E., Kesson S. E., Ware N. G., Hibberson W., and Major A. (1979) Immobilisation of high level nuclear reactor wastes in SYNROC. *Nature* **278**, 219–223.

Ringwood A. E., Kesson S. E., Reeve K. D., Levins D. M., and Ramm E. J. (1988) SYNROC. In *Radioactive Waste Forms for the Future* (eds. W. Lutze and R.C. Ewing). North Holland, Amsterdam, pp. 233–333, Chapter 4.

Roberts S. K., Bourcier W. L., and Shaw H. F. (2000) Aqueous dissolution kinetics of pyrochlore, zirconolite and brannerite at 25, 50, and 75 °C. *Radiochim. Acta* **88**, 539–543.

Schuiling R. D., and Vink B. W. (1967) Stability relations of some titanium-minerals (sphene, perovskite, rutile, anatase). *Geochim. Cosmochim. Acta* **31**, 2399–2411.

Stephan T. (2001) TOF-SIMS in cosmochemistry. *Planet. Space Sci.* **49**, 859–906.

Stoll W. (1998) What are the options for disposition of excess weapons plutonium? *Mater. Res. Soc. Bull.* **23**, 6–16.

Strachan D. M., Scheele R. D., Buck E. C., Icenhower J. P., Kozelisky A. E., Sell R. L., Elovich R. J., and Buchmiller W. C. (2005) Radiation damage effects in candidate titanates for pu disposition: Pyrochlore. *J. Nucl. Mater.* **345**, 109–135.

Swope R. J., Smyth J. R., and Larson A. C. (1995) H in rutile-type compounds: I. Single-crystal neutron and X-ray diffraction study of H in rutile. *Am. Mineral.* **80**, 448–453.

Weber W. J., Wald J. W., and Matzke H. (1986) Effects of self-radiation damage in Cm-doped $Gd_2Ti_2O_7$ and $CaZrTi_2O_7$. *J. Nucl. Mater.* **138**, 196–209.

Williams C. T., Wall F., Woolley A. R., and Phillipo S. (1997) Compositional variation in pyrochlore from the Bingo carbonatite, Zaïre. *J. Afr. Earth Sci.* **25**, 137–145.

Zhang Z., Li H., Vance E. R., McLeod T., and Scales N. (2004) Aqueous dissolution of pyrochlore and zirconolite in F–bearing solutions. In *Scientific Basis for Nuclear Waste Management XXVII*, vol. 824 (eds. J. M. Hanchar, S. Stroes-Gascoyne, and L. Browning). Materials Research Society, Warrendale, Pennsylvania.

Associate editor: Liane G. Benning